

Modulation mechanism of Mn-O strength in α -MnO₂ catalyst for high-efficiency catalytic combustion of propane

Shengnan Song^{a,b}, Meicheng Wen^{a,b}, Weinan Zhao^{a,b}, Jiejing Kong^{a,b}, Guiying Li^{a,b}, Taicheng An^{a,b,*}

^a Guangdong Key Laboratory of Environmental Catalysis and Health Risk Control, Guangdong-Hong Kong-Macao Joint Laboratory for Contaminants Exposure and Health, Institute of Environmental Health and Pollution control, Guangdong University of Technology, Guangzhou 510006, China

^b Guangdong Engineering Technology Research Center for Photocatalytic Technology Integration and Equipment, Guangzhou Key Laboratory of Environmental Catalysis and Pollution Control, School of Environmental Science and Engineering, Guangdong University of Technology, Guangzhou 510006, China



ARTICLE INFO

Keywords:

α -MnO₂
Mn-O strength
Propane
DFT calculations
Catalytic combustion

ABSTRACT

The cleavage of C-H with high energy impedes the catalytic combustion of propane. Herein, α -MnO₂ with modulation of Mn-O strength by changing the calcination temperature was applied in propane catalytic combustion. α -MnO₂ calcinated at 350 °C (α -MnO₂-350) exhibited superior performance ($T_{20}=150$ °C, $T_{90}=220$ °C) in propane oxidation due to the synergistic effect of oxygen vacancies (OVs) and Lewis acidity. Density functional theory (DFT) calculations revealed that the lowest o-vacancy formation energy on α -MnO₂-350 ($E_{vo}=0.74$ eV) with its lowest Mn-O strength prompted the existence of abundant OVs and propane oxidation. Moreover, the highest Lewis acidity in α -MnO₂-350 displayed the strongest propane adsorption, promoting the activation of C-H. The mineralization of propane on α -MnO₂-350 dropped steeply after 68 h while could recover to 90 % in long-term water vapor stability test owing to the H₂O adsorbed at OVs and the carbonaceous intermediates adsorbed at the Lewis acid sites.

1. Introduction

As the important air pollutants, even a lower concentration of volatile organic compounds (VOCs) will cause a serious threat to human health and environment [1,2]. More attention has been focused on the light alkanes owing to their wide emission in vehicles, petrochemicals, and power plants [3]. Propane as the typical light alkane is quite difficult to degrade due to the high thermal and chemical stability of its saturated C-H bonds [4]. Besides, the first C-H activation is regarded as the rate-controlling step during the propane oxidation [5]. Therefore, the removal of propane has been considered as a huge challenge.

Catalytic combustion is widely applied in the degradation of VOCs, and much effort has been devoted to the development of catalysts with high activity [6,7]. Although the supported noble metal catalysts are used for the catalytic combustion of propane due to their high activity, the high cost and high degradation temperature (> 300 °C) limit their application in the catalytic combustion of propane [8–10]. Among the transition metal oxides, manganese oxide has been proven to be a potential candidate to the catalytic combustion of VOCs, relating to its rich

content, low price, and the existence of Mn³⁺/Mn⁴⁺ [11,12]. It is well known that the manganese oxides contain different structures including α -, β -, γ -, and δ -MnO₂ structures under different synthetic conditions, and α -MnO₂ was found to exhibit the highest activity for propane combustion in contrast with γ -MnO₂, β -MnO₂ and δ -MnO₂, with T_{90} at 290 °C [13]. Besides, different kinds of methods have been investigated to improve the catalytic performance of α -MnO₂, including the variation of crystal facet [14], doping of heteroatom [15], and the modulation of morphologies [16]. However, the reported are mostly concentrated on the enhancement of O₂ activation to promote the oxidation of propane and less attention is paid on the effect of acidity of α -MnO₂ for propane catalytic combustion.

Generally, the highest occupied molecular orbitals (HOMOs) of light alkanes determine their catalytic oxidation performance due to that they provide electrons to the acid sites to be activated [4], and the HOMOs of light alkanes mainly distribute along the C-H bonds. Moreover, recent investigations indicated that the Lewis acid sites could promote C-H dissociation of alkanes. Yue et al. [17] stated that Sn-Beta zeolite with Lewis acid sites could activate the C-H bonds, thus showing high

* Corresponding author at: Guangdong Key Laboratory of Environmental Catalysis and Health Risk Control, Guangdong-Hong Kong-Macao Joint Laboratory for Contaminants Exposure and Health, Institute of Environmental Health and Pollution control, Guangdong University of Technology, Guangzhou 510006, China.

E-mail address: antc99@gdut.edu.cn (T. An).

catalytic activity in propane dehydrogenation. Tang et al. [18] found that Mg dopants in $\text{Co}_{1.5}\text{Mn}_{1.5}\text{O}_4$ spinel catalysts enhanced Lewis acidity of the catalysts which promoted efficient C-H dissociation of propane. Jian et al. [19] improved the Lewis acid sites of Co_3O_4 through varying its crystal facets to improve propane activation. The modulation of acidity in catalysts could efficiently enhance the activity to catalytic combustion of alkanes. OVs are quite important for the variation of geometrical and electronic structures as well as chemical properties of MnO_2 [20]. Most reported that the concentration of OVs contributed mostly to VOCs catalytic oxidation performances for manganese-based catalysts in that the adsorbed oxygen on OVs facilitated the reaction process. However, the Lewis acid sites of catalysts would increase with the existence of OVs owing to maintain electrostatic balance in the catalysts. Besides, the modification of metal-O strength would influence the surface electronic properties of transition metal oxide, thus affecting the existence of OVs [21]. Therefore, the construction of Lewis acid sites in MnO_2 by the modulation of Mn-O strength could be an underlying way to promote the activity to propane degradation.

In this work, a series of $\alpha\text{-MnO}_2$ with different Mn-O strength to modulate its acidity were fabricated by regulating calcination temperature. It was observed that $\alpha\text{-MnO}_2\text{-350}$ displayed the highest activity in propane oxidation in contrast with $\alpha\text{-MnO}_2\text{-270}$, $\alpha\text{-MnO}_2\text{-400}$ and $\alpha\text{-MnO}_2\text{-500}$. The higher amount of Lewis acidity, adsorbed oxygen species, and OVs was then measured to $\alpha\text{-MnO}_2\text{-350}$ catalyst with the lowest Mn-O strength demonstrated by the results of XPS, py-DRIFTS and Raman spectra. Moreover, catalytic activity over $\alpha\text{-MnO}_2\text{-350}$ in the catalytic combustion of ethane, propane, and n-butane was also comparably investigated, and the oxidation pathway of propane was proposed through the results of in situ diffused reflectance infrared Fourier transform spectra. It was found that the decrease of adsorbed oxygen species and the deposition of carbonaceous intermediates deactivated the activity of $\alpha\text{-MnO}_2\text{-350}$ in long-term water vapor stability test.

2. Experimental

2.1. Catalyst preparation and characterization

All the $\alpha\text{-MnO}_2$ catalysts were prepared by a mild hydrothermal method. Briefly, 17 mmol manganous nitrate (II) was added into 40 mL de-ionized water under magnetic stirring to form a homogeneous solution. Then, 19 mmol potassium permanganate was added into the aforementioned solution, stirring for 24 h at room temperature. The obtained mixture was transferred into the Teflon-lined autoclave, and heated at 70 °C for 24 h. After that, the dark brown product was collected by filtration and washed several times with anhydrous alcohol, and subsequently dried at 105 °C overnight. The dark brown product was then calcined at 270 °C, 350 °C, 400 °C and 500 °C for 2 h with a heating rate of 1 °C min⁻¹. These obtained products were named as $\alpha\text{-MnO}_2\text{-270}$, $\alpha\text{-MnO}_2\text{-350}$, $\alpha\text{-MnO}_2\text{-400}$, and $\alpha\text{-MnO}_2\text{-500}$, respectively.

The morphology, structure, and composition of the materials were characterized by transmission electron microscopy (TEM, 200 kV, Talos-F200x, FEI), X-ray diffraction (XRD, D8 ADVANCE, Bruker) and X-ray photoelectron spectroscopy (XPS, Escalab 250Xi, Thermo Fisher). The N₂ physisorption isotherms were measured at 77 K using an Autosorb iQ Station instrument (Quantachrome, America). Temperature programmed reduction of H₂ (H₂-TPR), temperature programmed desorption of O₂ (O₂-TPD), temperature programmed desorption of propane (propane-TPD) and temperature-programmed oxidation of O₂ (O₂-TPO) were carried out using an Autochem absorption analyzer (TP-5078, China). Thermogravimetric analysis (TGA) was conducted on a Thermogravimetric Analyzer (TGA2), at a rate of 10 °C min⁻¹ under nitrogen. Raman measurements were carried out on a confocal Raman Spectroscopy (LabRAM HR Evolution, HORIBA Jobin Yvon), and the wavelength was set as 532 nm. Diffuse reflectance infrared Fourier transform spectroscopy of pyridine adsorption (Py-DRIFTS) was

performed using a NICOLET 380 FT-IR spectrometer. In situ DRIFTS of propane was recorded on a Nicolet 6700 spectrometer equipped with a DRIFTS cell (Harrick) and a highly sensitive MCT detector cooled by liquid nitrogen at 600–4000 cm⁻¹ with 32 scans at a resolution of 4 cm⁻¹. The detailed characterization methods are described in the Supporting Information.

2.2. Catalysts activity test

Catalytic combustion of propane was carried out in a continuous flow fixed-bed tube microreactor (i.d. = 6 mm) equipped with a heating furnace under atmospheric pressure. 50 mg of the prepared samples was packed in the reactor. The reactant mixture consisted of 300 ppm propane/200 ppm ethane/200 ppm propane/200 ppm n-butane and 20 % O₂ balanced in N₂ with a total flow of 25 mL min⁻¹, corresponding to a weight hourly space velocity (WHSV) of 30,000 mL g⁻¹ h⁻¹. The VOC concentrations of the inlet and outlet were detected by the GC-9800 equipped with a flame ionization detector (FID). The CO₂ concentration was also analyzed on a GC9800 (FID, equipped with a Ni-catalyst-based methanizer) gas chromatography system. Propane conversion (X_p), ethane conversion (X_e), n-butane conversion (X_b), propane mineralization (X_m) and reaction rate r (mol⁻¹ g⁻¹ s⁻¹) were calculated as follows:

$$X_p = \frac{[C_3H_8]_{in} - [C_3H_8]_{out}}{[C_3H_8]_{in}} \times 100\%$$

$$X_e = \frac{[C_2H_6]_{in} - [C_2H_6]_{out}}{[C_2H_6]_{in}} \times 100\%$$

$$X_b = \frac{[C_4H_{10}]_{in} - [C_4H_{10}]_{out}}{[C_4H_{10}]_{in}} \times 100\%$$

$$X_m = \frac{[CO_2]_{out}}{3 \times ([C_3H_8]_{in} - [C_3H_8]_{out})} \times 100\%$$

$$r = \frac{X_p \times V \times [C_3H_8]_{in}}{m_{cat}}$$

where $[C_3H_8]_{in}$, $[C_2H_6]_{in}$, and $[C_4H_{10}]_{in}$ are the inlet concentration of propane, ethane, and n-butane, respectively. $[C_3H_8]_{out}$, $[C_2H_6]_{out}$, and $[C_4H_{10}]_{out}$ are the outlet concentration of propane, ethane, and n-butane, respectively. $[CO_2]_{out}$ is the outlet concentration of CO₂, V represents the total molar flow rate, and m_{cat} is the amount of the catalyst.

3. Results and discussion

3.1. Physical textural and surface properties of prepared catalysts

The crystal structure of the prepared materials was characterized by XRD (Fig. S1). All the prepared catalysts presented the (110), (200), (310), (211), (301), (411), (600), (521), (002), and (541) facets which were attributed to the tetragonal phase of $\alpha\text{-MnO}_2$ (JCPDS, PDF#44-0141) [13]. The obtained results suggested that the calcination temperature did not cause a transformation of the crystal structures of $\alpha\text{-MnO}_2$. The N₂ adsorption-desorption and pore size distribution of $\alpha\text{-MnO}_2\text{-270}$, $\alpha\text{-MnO}_2\text{-350}$, $\alpha\text{-MnO}_2\text{-400}$, and $\alpha\text{-MnO}_2\text{-500}$ were shown in Fig. S2, and their specific surface area, pore volume and average pore size were summarized in Table 1. All the catalysts exhibited a type IV adsorption isotherms with a hysteresis loop in the P/P₀ region above 0.8 and an H1 type hysteresis loop (Fig. S2a), indicating the mesoporous structure of the prepared catalysts. A peak around 2 – 4 nm was observed in the pore-size distribution curves, indicating the compaction of $\alpha\text{-MnO}_2$ nanocrystal. The surface areas of $\alpha\text{-MnO}_2\text{-350}$, $\alpha\text{-MnO}_2\text{-270}$, $\alpha\text{-MnO}_2\text{-400}$, and $\alpha\text{-MnO}_2\text{-500}$ were 58, 52, 54, and 48 m² g⁻¹, respectively. Besides, the pore volume and pore size of the prepared catalysts

Table 1

Textural parameters of the prepared catalysts.

Catalyst	specific surface areas ($\text{m}^2 \text{ g}^{-1}$)	Pore volume ($\text{cm}^3 \text{ g}^{-1}$)	Average pore diameter (nm)
$\alpha\text{-MnO}_2\text{-270}$	52	12.0	4.53
$\alpha\text{-MnO}_2\text{-350}$	58	13.4	4.06
$\alpha\text{-MnO}_2\text{-400}$	54	12.4	4.60
$\alpha\text{-MnO}_2\text{-500}$	48	11.1	4.39

were similar (Fig. S2b). Clearly, there is no obvious difference in the pore volume, surface area and pore size of the prepared catalysts, suggesting that the calcination temperature does not cause an obvious variation of the pore structure. The TEM images of $\alpha\text{-MnO}_2\text{-270}$, $\alpha\text{-MnO}_2\text{-350}$, $\alpha\text{-MnO}_2\text{-400}$, and $\alpha\text{-MnO}_2\text{-500}$ were also displayed in Fig. 1. It could be observed that all the prepared samples showed a rod-like morphology. The high-resolution TEM images of $\alpha\text{-MnO}_2\text{-270}$, $\alpha\text{-MnO}_2\text{-350}$, $\alpha\text{-MnO}_2\text{-400}$, and $\alpha\text{-MnO}_2\text{-500}$ were also examined (Fig. S3), and all exhibited a well-identified periodic lattice fringe of 0.24 and 0.69 nm, respectively, corresponding to interplanar distance of (110) facet of $\alpha\text{-MnO}_2$. The result suggests that the calcination temperature does not influence texture of prepared samples.

Raman spectra were applied to detect near-neighbor environment of oxygen coordination around Mn ions. As shown in Fig. 2a, the catalysts prepared at different calcination temperatures showed obvious Raman

peaks around 573 and 633 cm^{-1} , which were corresponded to the stretching vibration v_3 (Mn-O) of the $[\text{MnO}_6]$ basal plane and the symmetric stretching vibration v_2 (Mn-O) of the MnO_6 group, respectively [22]. In addition, a significant red shift of the Raman peak at 633 cm^{-1} was observed on $\alpha\text{-MnO}_2\text{-350}$ in contrast with $\alpha\text{-MnO}_2\text{-270}$, $\alpha\text{-MnO}_2\text{-400}$, and $\alpha\text{-MnO}_2\text{-500}$, which could be attributed to the crystal cell distortion and amorphous structural defects of the catalyst. Besides, the more the red shift, the weaker the Mn-O bond in the catalyst, suggesting that the weaker Mn-O bond may be attributed to the presence of abundant OVs in $\alpha\text{-MnO}_2\text{-350}$. The strength of Mn-O bond in prepared catalysts was evaluated by Mn-O force constant (k) calculated according to Hooke's law [14]. It was found that Mn-O force constant (k) increased in the sequence $\alpha\text{-MnO}_2\text{-350} < \alpha\text{-MnO}_2\text{-270} < \alpha\text{-MnO}_2\text{-400} < \alpha\text{-MnO}_2\text{-500}$ (Fig. 2b). The calculated Mn-O force constant could represent Mn-O bond strength, and a lower force constant means a weaker Mn-O bond strength. The obtained results revealed that $\alpha\text{-MnO}_2\text{-350}$ possessed the lowest Mn-O strength, thus prompting the existence of OVs.

The surface properties of prepared catalysts were investigated by XPS, and the detailed analysis results were displayed in Fig. 3 and Table 2. As shown in Fig. 3a, the Mn 2p3/2 spectra were resolved into two peaks with binding energy at 641.3 and 642.6 eV corresponding to Mn^{3+} and Mn^{4+} species, respectively [23,24]. The ratio of Mn^{3+} and Mn^{4+} was calculated by their peak areas and listed in Table 2. The $\text{Mn}^{3+}/\text{Mn}^{4+}$ ratios decreased as follow: $\alpha\text{-MnO}_2\text{-350} > \alpha\text{-MnO}_2\text{-270} > \alpha\text{-MnO}_2\text{-400} > \alpha\text{-MnO}_2\text{-500}$. It is said that OVs will be generated to maintain electrostatic balance once Mn^{3+} appears in the catalysts [25]. A higher ratio of $\text{Mn}^{3+}/\text{Mn}^{4+}$ means the higher content of OVs as the

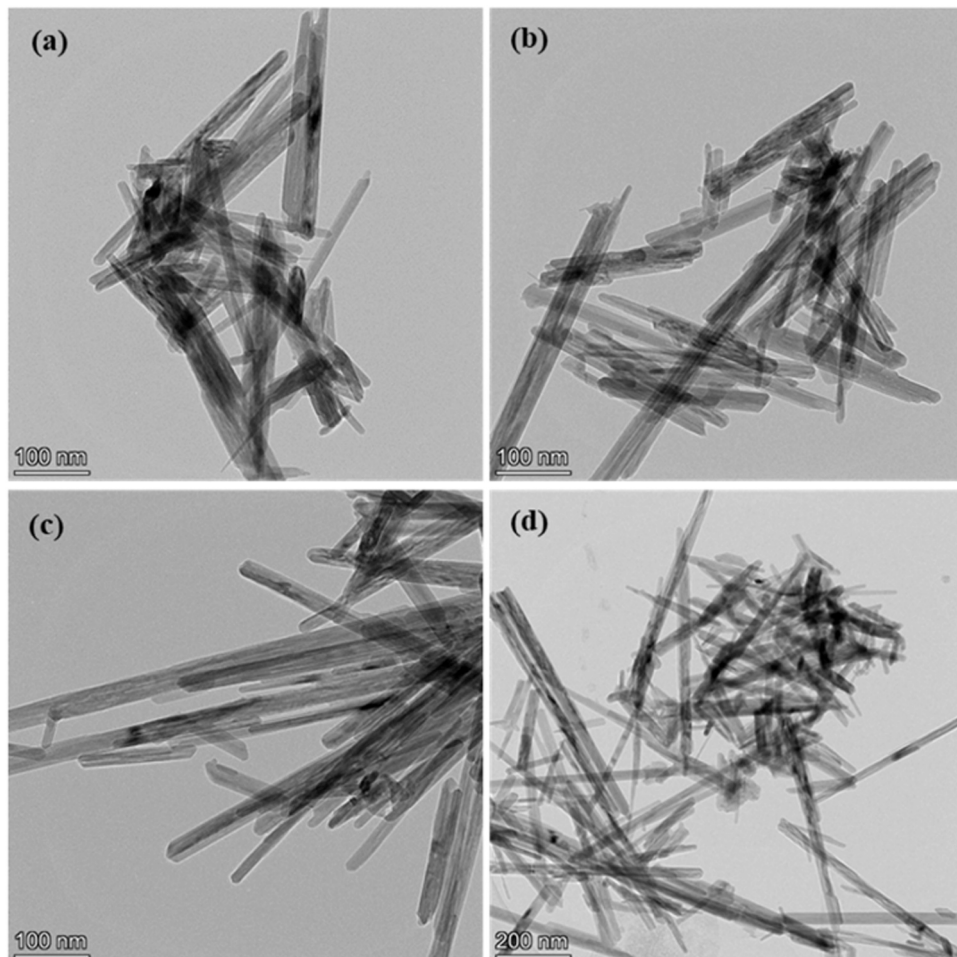


Fig. 1. TEM images of $\alpha\text{-MnO}_2\text{-270}$ (a), $\alpha\text{-MnO}_2\text{-350}$ (b), $\alpha\text{-MnO}_2\text{-400}$ (c), and $\alpha\text{-MnO}_2\text{-500}$ (d) catalysts.

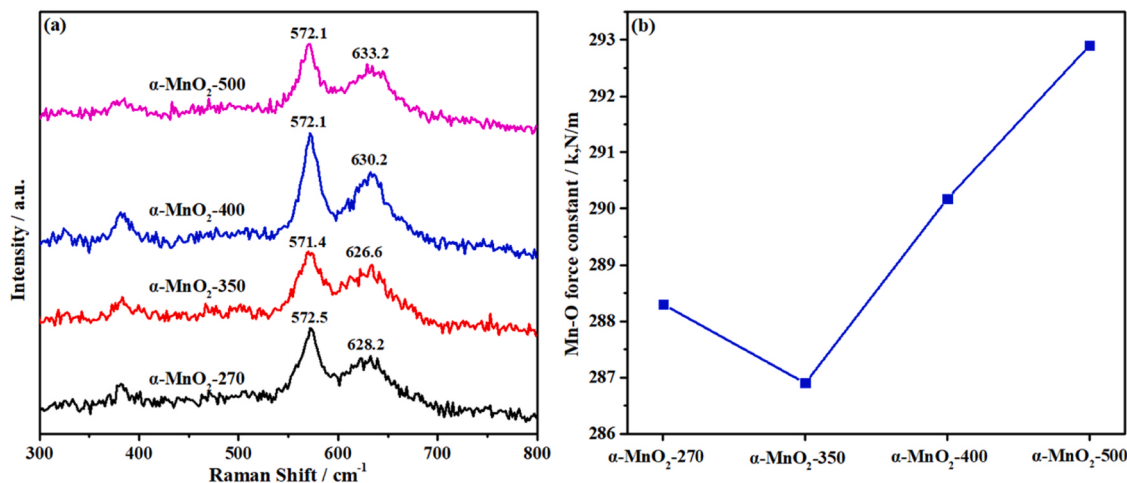


Fig. 2. Raman spectra of α -MnO₂-270, α -MnO₂-350, α -MnO₂-400, and α -MnO₂-500 catalysts.

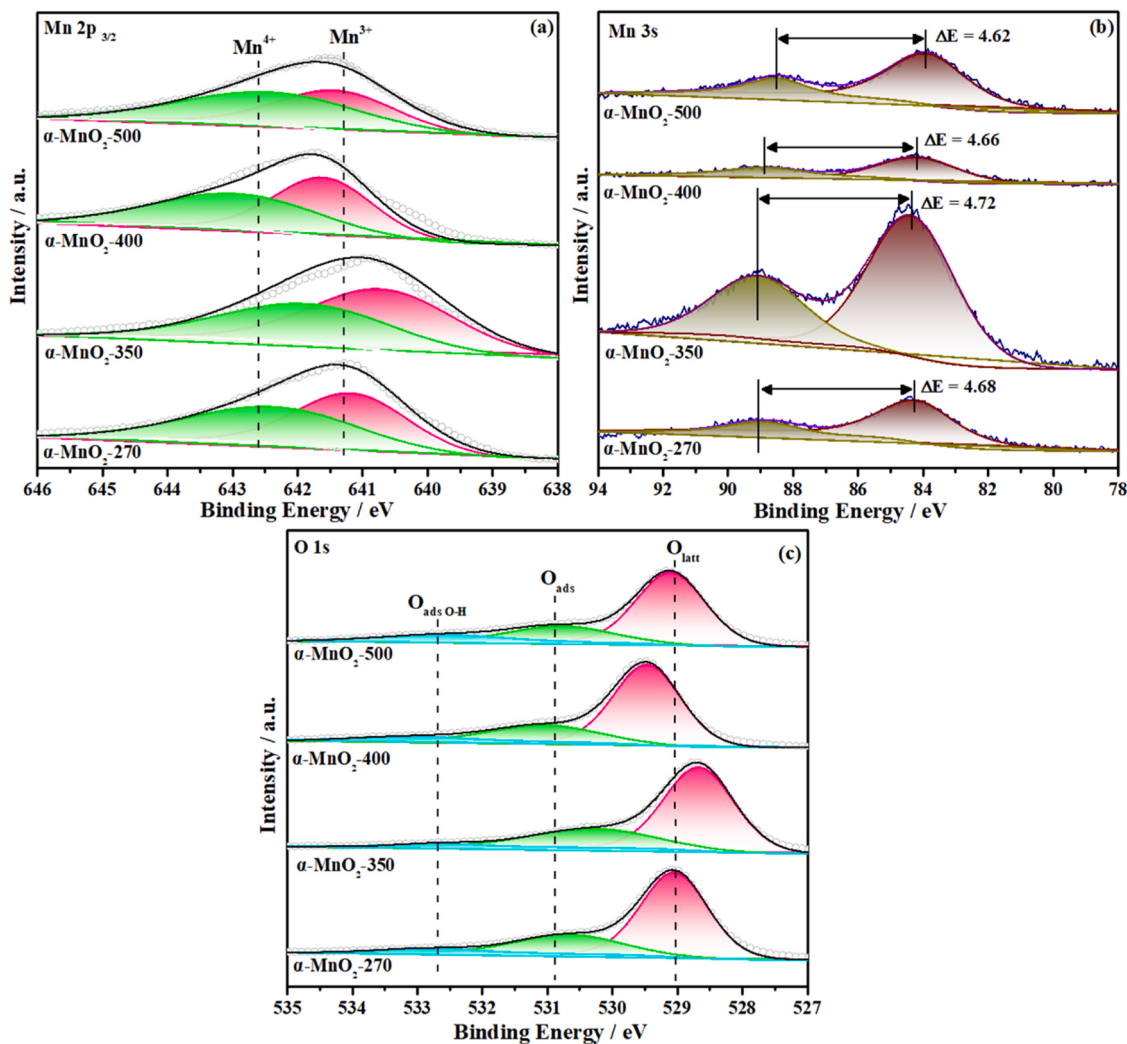


Fig. 3. XPS spectra of Mn 2p (a), Mn 3 s (b) and O 1 s (c) for α -MnO₂-270, α -MnO₂-350, α -MnO₂-400, and α -MnO₂-500 catalysts.

active sites in the oxidation process. Thus, α -MnO₂-350 possessed the highest amount of OV due to its highest Mn³⁺/Mn⁴⁺ ratio. The average oxidation state (AOS) of Mn in the catalysts was also calculated according to the binding energy difference between two peaks in Mn 3 s XPS spectra (Fig. 3b). The AOS of α -MnO₂-270, α -MnO₂-350,

α -MnO₂-400, and α -MnO₂-500 was obtained as 3.69, 3.64, 3.71 and 3.75, respectively. The lowest surface AOS in α -MnO₂-350 represented the largest amount of Mn species in lower valance (Mn³⁺) on surface of α -MnO₂-350, which was beneficial to the generation of OV in order to maintain the charge balance. Moreover, as the antibonding e_g^1 electron

Table 2
XPS analysis of the prepared catalysts.

Catalyst	O 1 s			Mn 2p			AOS ^a
	O _{ads} (%)	O _{lat} (%)	O _{ads} /O _{lat} (%)	Mn ³⁺ (%)	Mn ⁴⁺ (%)	Mn ³⁺ /Mn ⁴⁺ (%)	
α-MnO ₂ -270	25.9	74.1	34.9	50.0	50.0	1.00	3.69
α-MnO ₂ -350	28.7	71.3	40.2	56.3	43.7	1.29	3.64
α-MnO ₂ -400	25.2	74.8	33.6	49.8	50.2	0.99	3.71
α-MnO ₂ -500	24.7	75.3	32.8	44.3	55.7	0.80	3.75

^a AOS was calculated by formula: AOS = 8.956–1.126ΔEs, where ΔEs represented the difference of binding energies between two Mn 3 s peaks.

of Mn³⁺ ($t_{2g}^3e_g^1$) leads to longer Jahn-Teller distorted and weaker Mn-O bonds than Mn⁴⁺ [26], thereby α-MnO₂-350 catalyst with the highest Mn³⁺/Mn⁴⁺ ratio possessed the lowest Mn-O strength, which was consistent with the result of Raman analysis.

The O 1 s spectra in Fig. 3c could be deconvoluted into three peaks at 529.0, 530.9 and 532.7 eV. The peaks at 529.0 and 532.7 eV could be attributed to the lattice oxygen (O_{latt}), and surface hydroxyl oxygen (O_{ads} O-H), respectively [27], while the peak centered at 530.7 eV could be attributed to the oxygen species chemisorbed at OVs over catalysts (O_{ads}) [28]. O_{ads} were regarded as active oxygen species due to their high activity, which promoted the adsorption and activation of oxygen and the replenish of lattice oxygen [14]. As listed in Table 2, α-MnO₂-350 showed the highest amount of O_{ads}/O_{latt}, indicating that it possessed the highest amount of OVs on its surface, which was attributed to that the release of oxygen in α-MnO₂-350 with highest Mn³⁺/Mn⁴⁺ ratio was facilitated as the weaker bond energy of Mn(III)-O in contrast with Mn(IV)-O. Thus, α-MnO₂-350 catalyst with the lowest Mn-O strength exhibited the highest amount of O_{ads} and OVs.

The results of Raman and XPS suggested that the α-MnO₂ calcinated at 350 °C and 500 °C possessed the lowest Mn-O strength and highest Mn-O strength, respectively. That is due to that the calcination temperature influences the release of O₂ accompanied with the existence of Mn³⁺ on the catalysts surface, thus leading to the weak Mn-O strength of the catalysts as the antibonding e_g^1 electron of Mn³⁺ ($t_{2g}^3e_g^1$) induces longer Jahn-Teller distorted and weaker Mn-O bonds than Mn⁴⁺. DFT calculation was adopted to understand the effects of difference of Mn-O

strength in α-MnO₂ on the formation of oxygen vacancy. We calculated the formation energies of a single O vacancy at the surface of α-MnO₂, and the results were shown in Fig. 4. Note that the lower the formation energy of oxygen vacancy, the easier the forming of oxygen vacancy. It is found that the formation energy of oxygen vacancy for α-MnO₂-350 with low Mn-O strength (E_{ov} = 0.74 eV) was much lower than α-MnO₂-500 with high Mn-O strength (E_{ov} = 1.85 eV), indicating that it was easier to form OVs on α-MnO₂ surface with lower Mn-O strength, and α-MnO₂-350 with low Mn-O strength should possess more OVs than α-MnO₂-500. The theoretical result conducted by ourself is also consistent with the above-mentioned results of Raman and XPS.

3.2. Redox properties and oxygen mobility of prepared catalysts

The measurement of H₂-TPR was conducted for insight into the reducibility of prepared samples. It could be obviously seen from Fig. 5a that two reduction peaks appeared in prepared catalysts at 100–200 °C and 300–400 °C, which were attributed to the reduction of the surface active oxygen species [29] and the reduction of MnO₂ to Mn₂O₃, respectively [30]. α-MnO₂-350 catalyst displayed the lowest reduction temperature of active surface oxygen at 253 °C, followed by α-MnO₂-270 (263 °C), α-MnO₂-400 (273 °C), and α-MnO₂-500 (278 °C). Besides, the reduction temperature of MnO₂ to Mn₂O₃ of α-MnO₂-270, α-MnO₂-350, α-MnO₂-400, and α-MnO₂-500 was 321 °C, 319 °C,

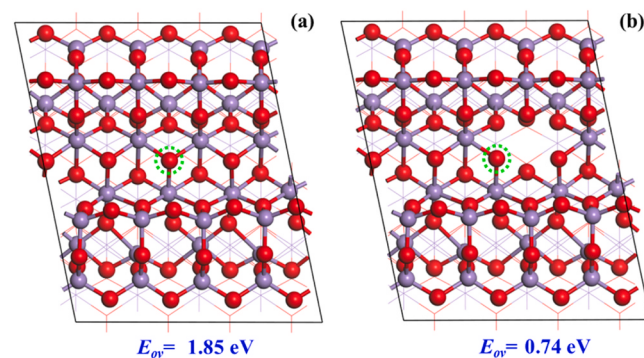


Fig. 5. Top view of formation energy of oxygen vacancy on α-MnO₂-500 with high Mn-O strength (a) and α-MnO₂-350 with low Mn-O strength (b) (Red: O atoms; Purple: Mn atoms; Green circle with dash line: oxygen vacancy).

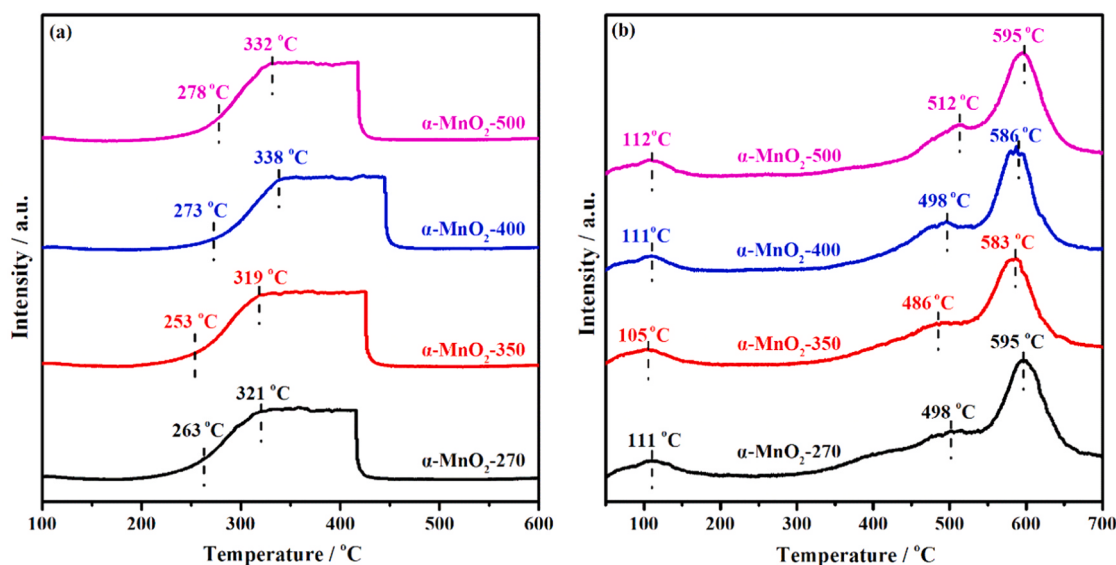


Fig. 4. H₂-TPR (a) and O₂-TPD (b) profiles of α-MnO₂-270, α-MnO₂-350, α-MnO₂-400, and α-MnO₂-500 catalysts.

338 °C, and 332 °C, respectively. It could be obtained that α -MnO₂-350 showed a reduction peak at the lowest temperature, indicating the most mobile oxygen species both at the surface and in the bulk, thus favorable for the mobility of oxygen species.

The O₂-TPD was also performed to investigate the surface oxygen species in prepared catalysts. As depicted in Fig. 5b, the O₂ desorption peak could be divided into low-temperature (<150 °C) desorption peak, medium desorption peak (400–550 °C) and high-temperature peaks (>550 °C), which were attributed to the surface adsorbed oxygen species, surface lattice oxygen species, and bulk lattice oxygen, respectively [31]. It could be observed that α -MnO₂-350 catalyst showed the lowest desorption temperature of surface adsorbed oxygen and surface lattice oxygen, followed by α -MnO₂-270, α -MnO₂-400 and α -MnO₂-500, implying the enhanced oxygen mobility of α -MnO₂-350 catalyst. These results indicated that α -MnO₂-350 with the lowest Mn-O strength can enhance its reducibility and oxygen mobility, thus prompting the oxidation of propane. Fig. 5

3.3. Adsorption performance of propane on prepared catalysts

As considerable adsorption of reactant is beneficial to obtain a better catalytic activity, the temperature programmed desorption of propane is applied to investigate the effect of calcination temperature of the catalysts on the adsorption performance. As shown in Fig. 6a, it is obviously observed that the prepared catalysts displayed evident differences on account of propane adsorption. Notably, there were two desorption peaks of propane, centered around 60 °C and 110 °C which were attributed to physisorbed and chemisorbed propane, respectively. The α -MnO₂-350 catalyst possessed the highest desorption temperature of propane at 114 °C, as compared with α -MnO₂-270 (110 °C), α -MnO₂-400 (108 °C), and α -MnO₂-500 (106 °C), suggesting α -MnO₂-350 catalyst exhibited the strongest adsorption of propane and the strongest interaction with propane. To more intuitively demonstrate the strong adsorption of propane in α -MnO₂-350 catalyst, the most stable mode of propane adsorption on the surface of α -MnO₂-350 catalyst with low Mn-O strength and α -MnO₂-500 catalyst with high Mn-O strength and the corresponding adsorption energies were shown in Fig S4. The propane adsorption energy of α -MnO₂-350 and α -MnO₂-500 with oxygen vacancies was -0.97 eV and -0.78 eV, respectively. As a more negative adsorption energy indicated that the adsorption system was more thermodynamically stable. Thus, α -MnO₂-350 with low Mn-O strength displayed a stronger adsorption of propane, which was consistent with the propane-TPD analysis.

The acidity of catalyst could facilitate VOCs adsorption and C-H bond

activation, which played a vital role in VOCs oxidation. The surface acidity of the catalysts was investigated by py-DRIFTS as shown in Fig. 6b. All the catalysts showed four peaks. The peaks at 1445, 1605, and 1545 cm⁻¹ were attributed to the Lewis acid sites and Bronsted acid sites, respectively [7]. While, the peak at 1490 cm⁻¹ was attributed to that pyridine molecule coordinated with the Lewis and Bronsted acid sites. It could be observed that the peak area and intensity of Lewis acid site were higher than that of Bronsted acid sites, suggesting that all prepared catalysts predominantly comprised the Lewis acid sites. Besides, the acid sites peak area of α -MnO₂-350 was higher than those of α -MnO₂-270, α -MnO₂-400, and α -MnO₂-500. The quantitative data of acid sites obtained at 150 °C were listed in Table 3 to intuitively compare the surface acidity. The obtained result showed that α -MnO₂-350 possessed the highest amount of Lewis acid sites, followed by α -MnO₂-270, α -MnO₂-400, and α -MnO₂-500, which could be attributed to that α -MnO₂-350 with the lowest Mn-O bond strength possessed the highest amount of OV thus facilitating the increase of Lewis acidity in order to maintain the electrostatic balance. Combing the results of propane-TPD, DFT calculations of propane adsorption with py-DRIFT, α -MnO₂-350 catalyst possessed the strongest interaction with propane which could be attributed to its highest amount of Lewis acid sites. The HOMOs of light alkanes mainly distributed along the C-H bonds and provided electrons to the Lewis acid sites, thus the α -MnO₂-350 catalyst with highest Lewis acidity could promoted the adsorption of propane. Besides, the existence of Lewis acidity could accelerate the H-abstraction process [32], thus, the C-H activation of the adsorbed propane could be promoted. These obtained results suggested that the strongest interaction between propane and α -MnO₂-350 catalyst was attributed to the weakening of Mn-O bond strength, thus facilitating the adsorption and activation of propane.

Table 3
Quantification of surface acid sites on the catalysts by py-DRIFTS at 150 °C.

Sample	C _{Bronsted} ($\mu\text{mol g}^{-1}$)	C _{Lewis} ($\mu\text{mol g}^{-1}$)	C _{total} ($\mu\text{mol g}^{-1}$)	C _{Lewis} /C _{total} (%)
α -MnO ₂ -270	0.6	12.9	13.5	95.5
α -MnO ₂ -350	0.8	43.4	44.2	98.2
α -MnO ₂ -400	0.6	9.4	9.9	94.9
α -MnO ₂ -500	0.5	9.0	9.5	94.7

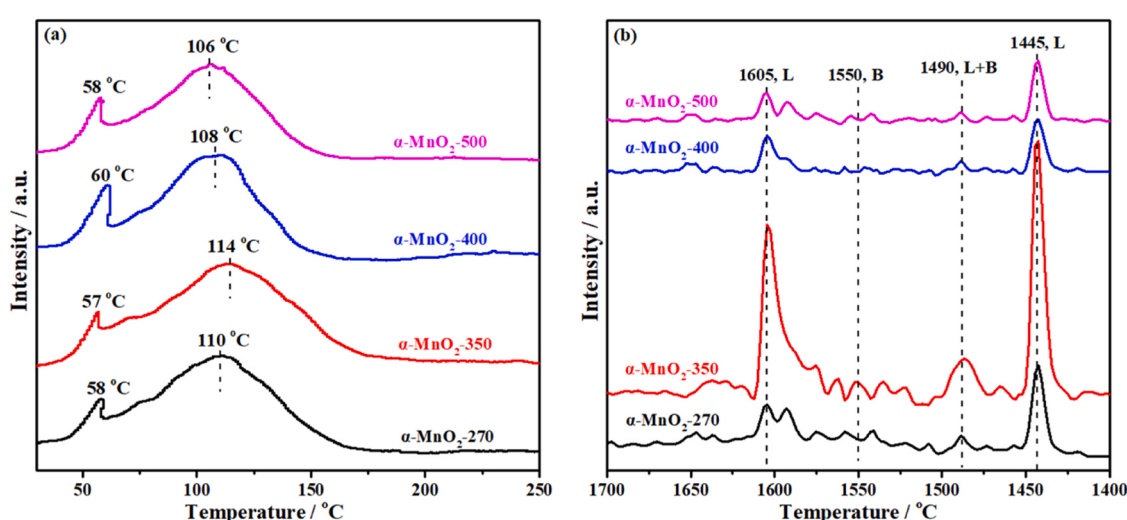


Fig. 6. Propane-TPD profiles (a) and py-DRIFTS at 150 °C (b) over α -MnO₂-270, α -MnO₂-350, α -MnO₂-400, and α -MnO₂-500 catalysts.

3.4. Catalytic activity and mechanism of prepared catalysts

The activities of $\alpha\text{-MnO}_2$ -270, $\alpha\text{-MnO}_2$ -350, $\alpha\text{-MnO}_2$ -400, and $\alpha\text{-MnO}_2$ -500 catalysts were evaluated in catalytic combustion of propane. Fig. 7a showed the conversion of propane as the function of reaction temperature. All prepared catalysts showed a high activity for the catalytic combustion of propane, with a conversion higher than 90% below 230 °C. To evaluate the comparison of catalytic activity of all prepared catalysts, the T_{20} and T_{90} were calculated (Table 4). The T_{20} and T_{90} of the catalysts were increased in the following order: $\alpha\text{-MnO}_2$ -350 ($T_{20}=150$ °C, $T_{90}=220$ °C) < $\alpha\text{-MnO}_2$ -270 ($T_{20}=153$ °C, $T_{90}=224$ °C) < $\alpha\text{-MnO}_2$ -400 ($T_{20}=157$ °C, $T_{90}=226$ °C) < $\alpha\text{-MnO}_2$ -500 ($T_{20}=164$ °C, $T_{90}=229$ °C), which suggested that the calcination temperature of the catalysts influenced their catalytic activity. The mineralization efficiencies were similar to the conversion of propane at the same temperature on $\alpha\text{-MnO}_2$ -350 catalyst (Fig. S5), indicating that $\alpha\text{-MnO}_2$ -350 displayed the highest catalytic performance and complete conversion of CO₂. On account of transition metal oxides, the surface oxygen species are closely related to the catalytic activity, which can crucially affect the catalytic process [33]. We also investigated the relationship of the O_{ads} content and the T_{20} . As shown in Fig. S6, the O_{ads} content of prepared catalysts reduced in the order $\alpha\text{-MnO}_2$ -350 > $\alpha\text{-MnO}_2$ -270 > $\alpha\text{-MnO}_2$ -400 > $\alpha\text{-MnO}_2$ -500. Inversely, the T_{20} exhibited the opposite trend. It can be seen that the catalytic activity is correlated to the O_{ads} content of the catalysts. The apparent activation energy (Ea) at the conversion below 20% of prepared catalysts was calculated by linear-fitting Arrhenius equation (Fig. 7b). The calculated apparent activation energy (Ea) value of $\alpha\text{-MnO}_2$ -350 (56.2 KJ mol⁻¹) was

Table 4
Catalytic properties of the prepared catalysts.

Catalyst	T_{20} (°C) ^a	T_{90} (°C) ^a	$r (\times 10^{-8} \text{ mol g}^{-1} \text{ s}^{-1})^b$	$C_3\text{H}_8$ conversion (°C) ^b	Ea (KJ mol ⁻¹) ^c
$\alpha\text{-MnO}_2$ -270	153	224	1.69	15.1	60.9
$\alpha\text{-MnO}_2$ -350	150	220	1.95	17.5	56.2
$\alpha\text{-MnO}_2$ -400	157	226	1.38	12.4	62.7
$\alpha\text{-MnO}_2$ -500	164	229	0.98	8.8	65.0

a: T_{20} and T_{90} represent the temperatures for 20 % and 90 % conversion of propane, respectively. b: Data obtained at 140 °C. c: The activation energies of the samples were calculated by Arrhenius equation: $k = Ae^{-E_a/RT}$.

considerably lower than those of $\alpha\text{-MnO}_2$ -270 (60.9 KJ mol⁻¹), $\alpha\text{-MnO}_2$ -400 (62.7 KJ mol⁻¹) and $\alpha\text{-MnO}_2$ -500 catalysts (65.0 KJ mol⁻¹); this result was in contrast to the order of the catalytic activity, suggesting that $\alpha\text{-MnO}_2$ -350 catalyst showed the highest activity and weakest Ea for propane oxidation. The reaction rate was also calculated in Table 4 to better comprehend the intrinsic activity of the catalysts. It was obviously observed that the reaction rate of $\alpha\text{-MnO}_2$ -350 ($1.95 \times 10^{-8} \text{ mol g}^{-1} \text{ s}^{-1}$) was higher than that of $\alpha\text{-MnO}_2$ -270 ($1.69 \times 10^{-8} \text{ mol g}^{-1} \text{ s}^{-1}$), $\alpha\text{-MnO}_2$ -400 ($1.38 \times 10^{-8} \text{ mol g}^{-1} \text{ s}^{-1}$) and $\alpha\text{-MnO}_2$ -500 ($0.98 \times 10^{-8} \text{ mol g}^{-1} \text{ s}^{-1}$). These obtained results suggested that $\alpha\text{-MnO}_2$ -350 catalyst really displayed the highest activity and the weakest apparent activation energy in propane

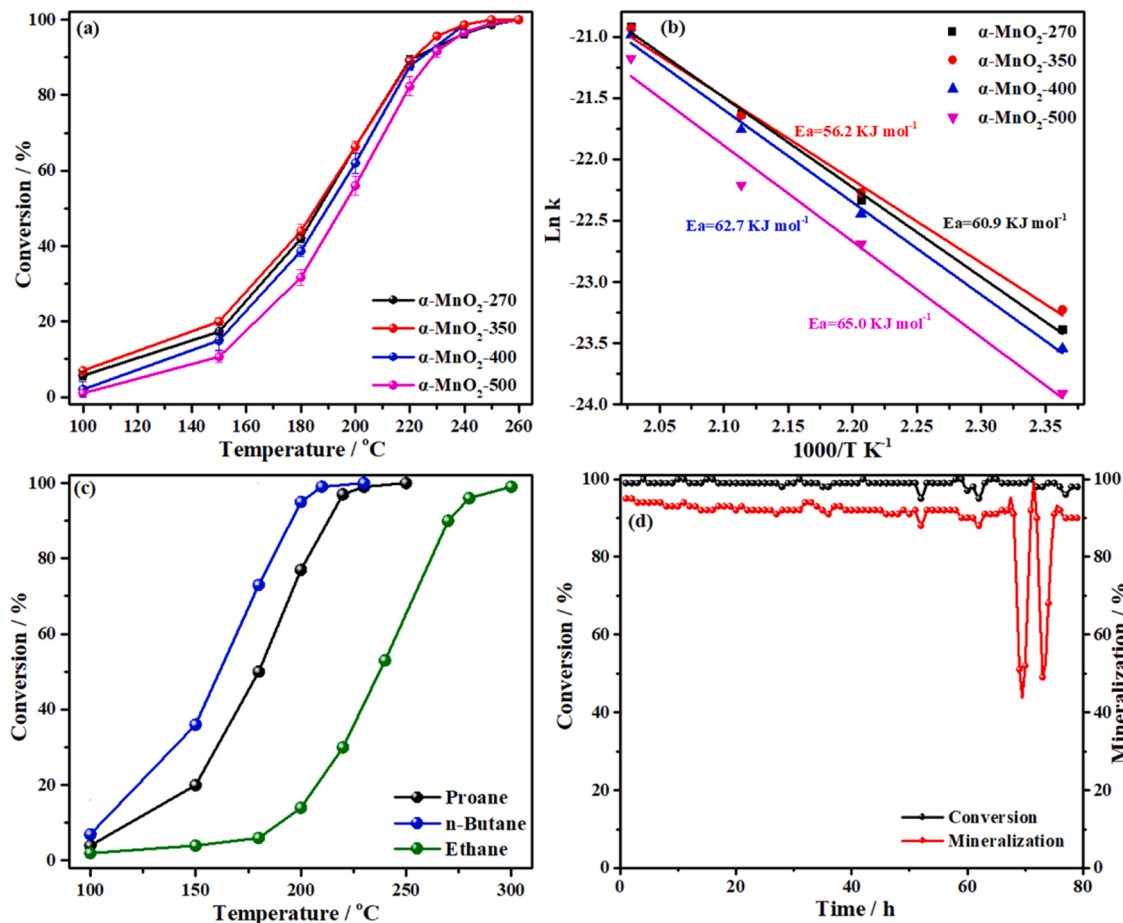


Fig. 7. Catalytic performance for 300 ppm propane as a function of temperature over the prepared catalysts (a), Arrhenius plots over the prepared catalysts (b), catalytic performances as a function of temperature during ethane (200 ppm), propane (200 ppm), and n-butane (200 ppm) combustion over $\alpha\text{-MnO}_2$ -350 catalyst at GHSV = 30,000 mL h⁻¹ g⁻¹ (c), water vapor resistance (5 vol%) tests for $\alpha\text{-MnO}_2$ -350 catalyst at 250 °C (d).

oxidation, and the activation and oxidation of propane was related to the calcination temperature of prepared catalysts.

We also investigated the applicability of α -MnO₂-350 catalyst for catalytic combustion of different kinds of VOCs, the catalytic performance of α -MnO₂-350 catalyst of ethane, propane, and n-butane was compared and shown in Fig. 7c and Table S1. Obviously, it was found that the complete conversion of ethane, propane, and n-butane could be achieved below 300 °C for degradation of different types of alkanes. The T₂₀ of n-butane was obtained as 122 °C, displaying 28 °C and 85 °C lower than that of propane and ethane, respectively (Table S1). As activation of C-H bond is the rate-determining step for alkanes combustion and once the first C-H bond is broken then the formation of carbon dioxide occurs easily, thus combustion of alkanes is closely related to the cleavage energy of its weakest C-H bonds. The C-H bond energy of secondary carbons (401 KJ mol⁻¹) is lower than primary carbons (420 KJ mol⁻¹) [34]. Consequently, n-butane with two secondary carbons was easier to degrade than propane with one secondary carbon, and propane was easier to degrade than ethane with two primary carbons, resulting the degradation of n-butane was easier than that of propane and ethane. These results suggest that α -MnO₂-350 catalyst exhibits the excellent catalytic performance for different types of alkanes, and alkane with shorter carbon chain is more difficult to be degraded.

In order to deeply understand the reaction mechanism, the temperature-dependent *in situ* DRIFTS was used to determine the reaction intermediates on α -MnO₂-350 catalyst in the process of propane catalytic combustion and reveal the possible catalytic reaction pathway, and the results were shown in Fig. 8. In general, the band at 2965 cm⁻¹ was assigned to C-H stretching vibration peaks of CH_n of propane [16], indicating the physisorbed propane through methyl C-H activation. An obvious characteristic peak of CO₂ (2360 cm⁻¹) [35] became more obvious with the increase of degradation temperature. That suggests that propane can be completely oxidized to CO₂ on the catalyst. The peaks at 1655 cm⁻¹, 1630 cm⁻¹ and 1470 cm⁻¹ were characteristic peaks of C=C bond and C-H bond of propylene, respectively [36,37]. Besides, the band at 1337 cm⁻¹ suggested the generation of propylene [37]. The peaks at 1586, 1371 cm⁻¹ and 1560, 1430 cm⁻¹ were attributed to characteristic peaks of formate species and acetate species [4,37,38], respectively. The peak of acrylate species was found at 1527 cm⁻¹ ($\nu_{as}(\text{COO})$) [4]. The peaks attributed to bidentate species (1315 cm⁻¹) and C-O bond (1281 cm⁻¹) were also detected [36,37]. Based on above results, it is speculated that possible reaction pathway of propane on the catalyst is as follows: firstly, the adsorbed propane is oxidized to propylene by its oxidative dehydrogenation on Lewis acid sites on α -MnO₂-350 catalyst as alkane is prone to generate alkene with the role of Lewis acidity [17]. Then the generated propylene is oxidized

to acrylate species by the active oxygen species of catalyst, and further oxidized to carbonate species (acetic acid and formic acid). The reaction mechanism of propane in the prepared catalysts should follow MVK mechanism due to the existence of OVs and surface lattice oxygen, that is, propane is gradually oxidized by the surface lattice oxygen, and the consumed surface lattice oxygen is replenished by the reactive oxygen species (ROSSs) generated by the activation of gaseous oxygen on the OVs. On the basis of the results of Raman, O₂-TPD, XPS, and DFT calculations, the α -MnO₂-350 catalyst with the lowest Mn-O strength possesses the highest ratio of Mn³⁺/Mn⁴⁺ and abundant OVs. Thus, the surface lattice oxygen is easier to release on the α -MnO₂-350 catalyst due to its lowest Mn-O strength and the existence of abundant OVs in α -MnO₂-350 catalyst promotes the adsorption and activation of O₂ to replenish the surface lattice oxygen. Moreover, the dissociation of adsorbed propane on the catalyst surface is regarded as the first step of the catalytic cycle in the catalytic combustion of propane based on the MVK mechanism. The results of py-DRIFTS, propane-TPD and DFT calculations of propane adsorption reveal that the adsorption and activation of propane are obviously improved in α -MnO₂-350 due to its highest Lewis acidity. Thus, the α -MnO₂-350 with the lowest Mn-O strength possesses the better catalytic activity for propane catalytic combustion due to the synergistic effect of OVs and Lewis acidity.

3.5. Stability tests of prepared catalyst

The stability of α -MnO₂-350 catalyst was investigated by recycling catalyst after the oxidation of propane under the same conditions and shown in Fig. S7. α -MnO₂-350 catalyst did not show significant loss in activity after three heating and cooling cycles, suggesting its excellent thermal stability. Considering that the water vapor always exists in real exhausts, the influence of humidity on the catalytic activity of α -MnO₂-350 catalyst was investigated. As shown in Fig. 7d, the conversion of propane maintained almost 100 % during 68-h long-term test under 5 vol% water vapor steam over α -MnO₂-350 catalyst. Conversely, its mineralization efficiencies dropped steeply after 68-h long-term test and could recover to 90 %. These results indicated that α -MnO₂-350 catalyst did not show an excellent water resistance in propane catalytic oxidation. To get deep insights into the deactivation mechanism of catalysts, we design a series of characterizations to investigate the variations during long-term test of propane oxidation under 5 vol% water vapor steam over α -MnO₂-350 catalyst.

In order to explore the changes of the surface structure during hydrothermal stability test, the XPS spectra of α -MnO₂-350 catalyst before and after deactivation were carried out comparably, and the results were shown in Fig. 9. The C1s-XPS of used α -MnO₂-350 catalyst were analyzed (Fig. 9a), and it was found that used α -MnO₂-350 catalyst exhibited three peaks at 284.8, 285.8, and 288.5 eV assigned to sp²C (C-C=C), sp³C(C-O), and oxidized C(C=O), respectively, according to the early reference [39]. Besides, the contents of C-O and C=O were obtained as 23.5 % and 9.12 %, respectively (Table S2), and the generated C-O and C=O on the surface of the used α -MnO₂-350 catalyst may be attributed to carbonaceous intermediates formed during the combustion reaction. A detailed analysis of the distribution of Mn in various valence states and O in different binding states before and after the deactivation (Fig. 9b-c, Table S2) showed that the content of Mn⁴⁺ increased significantly after the reaction (from 43.7 % to 66.2 %). While the content of O_{ads} decreased significantly after the reaction (from 28.7 % to 14.9 %). In addition, it could be seen that the binding energy of Mn and O moved to a higher binding energy, while the binding energy of C moved to a lower binding energy (Fig. S8). It could be rational to speculate that H₂O was adsorbed on the OVs, thus occupying the necessary vacancy for the activation of O₂ [12]. Besides, the carbonaceous intermediates were conjectured to be adsorbed at Lewis acid sites which could accelerate the process of polymerization thus forming the carbonaceous deposition [40]. Thus, the occupation of OVs and generation of carbonaceous intermediates impeded the oxidation of propane

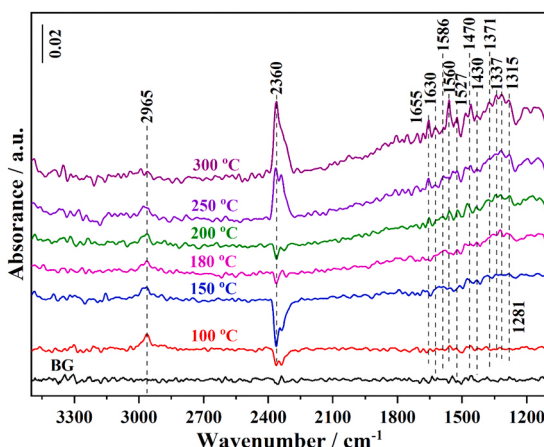


Fig. 8. In-situ DRIFTS spectra of propane oxidation (1000 ppm C₃H₈/Air) on α -MnO₂-350 catalyst.

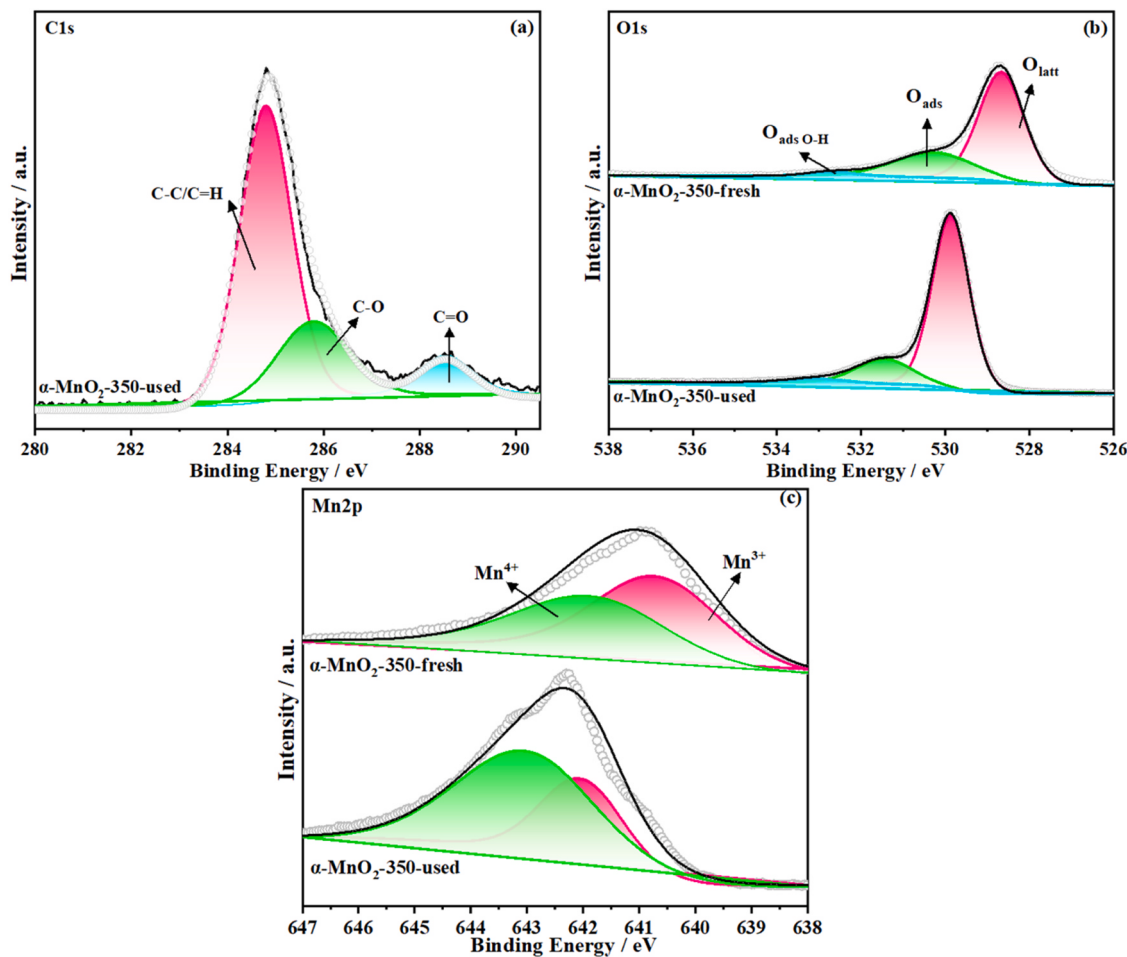


Fig. 9. XPS spectra of C1 s for the used $\alpha\text{-MnO}_2\text{-350}$ catalyst (a) and O1s (b), Mn2p (c) for the fresh and used $\alpha\text{-MnO}_2\text{-350}$ catalyst.

and caused the decrease of the catalytic performance of $\alpha\text{-MnO}_2\text{-350}$ catalyst during long-term water vapor reaction.

The deactivation of $\alpha\text{-MnO}_2\text{-350}$ catalyst was also analyzed by TG on catalysts before and after the reaction under nitrogen atmosphere, and the results were shown in Fig. S9. It could be observed that under N_2 atmosphere, the thermal decomposition profile showed three apparent mass loss at below 150 °C, 400–600 °C and 600–800 °C. The mass loss below 150 °C is related to the removal of physically adsorbed water/combined water and the release of lattice oxygen on catalyst surface [41, 42], and the mass loss at 400–600 °C and 600–800 °C is attributed to the production of O_2 during the conversion of MnO_2 to Mn_2O_3 and the conversion of Mn_2O_3 to Mn_3O_4 , respectively [43]. It could be clearly found that the mass loss of used (8.95 %) was more than that of fresh catalyst (8.75 %) in the range of 400–800 °C, which may be due to the obvious increase of Mn^{4+} content in used catalyst. Besides, the mass loss of used $\alpha\text{-MnO}_2\text{-350}$ catalyst decreased more steeply than that of fresh one in the range of 100–800 °C, which was attributed to the decomposition of generated carbonaceous intermediates on the surface of $\alpha\text{-MnO}_2\text{-350}$ catalyst. This result is also demonstrated by $\text{O}_2\text{-TPD}$ experiments (Fig. S10). It could be observed that the used $\alpha\text{-MnO}_2\text{-350}$ catalyst showed an obvious peak at 99 °C, which may be caused by the oxidation of non-volatile organic compounds generated on the catalyst surface [44]. Another obvious peak (596 °C) and its surrounding shoulder peaks (518 °C, 552 °C) were mainly contributed to hard coke formed by polynuclear aromatic species [45]; the peaks at 342 °C and 437 °C were mainly attributed to the amorphous soft coke [46]. Therefore, the accumulation of these intermediates on the catalyst surface plays an important role in deactivation of the used catalyst during

long-term water vapor test.

Based on above results, it could be deduced that H_2O adsorbed on the OVs and the carbonaceous intermediates adsorbed at Lewis acid sites impeding the activation of O_2 and replenishment of surface lattice oxygen led to the deactivation of catalysts during long-term water vapor stability test. Therefore, improving water resistance of $\alpha\text{-MnO}_2$ catalyst could be achieved by stabilizing the existence of $\text{Mn}^{3+}/\text{Mn}^{4+}$ and introducing the sacrificial sites to inhibit the adsorption of water and carbonaceous intermediates on the active sites.

4. Conclusions

In this work, we modulated the Mn-O strength of $\alpha\text{-MnO}_2$ by the variation of calcination temperature to improve the performance in catalytic combustion of propane. $\alpha\text{-MnO}_2\text{-350}$ catalyst shows superior performance in catalytic combustion of propane as compared with $\alpha\text{-MnO}_2\text{-270}$, $\alpha\text{-MnO}_2\text{-400}$ and $\alpha\text{-MnO}_2\text{-500}$ catalyst, which is attributed to enhanced adsorption of propane, improved Lewis acidity and increased ROSs by the existence of OVs attributed to its lowest Mn-O strength. Besides, $\alpha\text{-MnO}_2\text{-350}$ catalyst displayed excellent catalytic activity to other kind alkanes such as ethane and n-butane combustion. Additionally, $\alpha\text{-MnO}_2\text{-350}$ catalyst showed slight deactivation phenomenon during long-term water vapor stability test caused by the occupation of OVs by adsorbed H_2O and the generation of carbonaceous intermediates at Lewis acid sites. This investigation proves that the modulation mechanism of Mn-O strength by changing the calcination temperature is feasible to achieve high activity for propane oxidation, while the formation of carbonaceous intermediates and decrease of

surface adsorbed oxygen species impede water vapor stability.

CRediT authorship contribution statement

Weina Zhao: Methodology, Investigation. **Meicheng Wen:** Writing – review & editing, Validation, Data curation. **Shengnan Song:** Writing – original draft, Methodology, Investigation, Formal analysis. **Taicheng An:** Writing – review & editing, Supervision, Funding acquisition, Conceptualization. **Guiping Li:** Writing – review & editing. **Jiejing Kong:** Validation, Data curation.

Declaration of Competing Interest

The authors declare that they have no known competing financial interests or personal relationships that could have appeared to influence the work reported in this paper

Data availability

No data was used for the research described in the article.

Acknowledgments

This work was financially supported by Research and Development Program Project of Key Areas of Guangdong Province (2019B110206002), National Natural Science Foundation of China (42377364, 42077332 and 42377099), Guangdong Provincial Natural Science Fund for Distinguished Young Scholars (2022B1515020051), and Science and Technology Project of Guangdong Province, China (2022-GDUT-A0007).

Appendix A. Supporting information

Supplementary data associated with this article can be found in the online version at [doi:10.1016/j.apcatb.2024.124120](https://doi.org/10.1016/j.apcatb.2024.124120).

References

- [1] T. Zhang, G. Li, Y. Yu, Y. Ji, T. An, Atmospheric diffusion profiles and health risks of typical VOC: numerical modelling study, *J. Clean. Prod.* 275 (2020) 122982.
- [2] Y. Ren, X. Guan, Y. Peng, A. Gong, H. Xie, S. Chen, Q. Zhang, X. Zhang, W. Wang, Q. Wang, Characterization of VOC emissions and health risk assessment in the plastic manufacturing industry, *J. Environ. Manag.* 357 (2024) 120730.
- [3] Q. Wu, J. Yan, M. Jiang, Q. Dai, J. Wu, M.N. Ha, Q. Ke, X. Wang, W. Zhan, Phosphate-assisted synthesis of ultrathin and thermally stable alumina nanosheets as robust Pd support for catalytic combustion of propane, *Appl. Catal. B: Environ.* 286 (2021) 119949.
- [4] T. Zhang, X. Lang, A. Dong, X. Wan, S. Gao, L. Wang, L. Wang, W. Wang, Difference of oxidation mechanism between Light C₃-C₄ alkane and alkene over mullite YMn₂O₅ oxides' catalyst, *ACS Catal.* 10 (2020) 7269–7282.
- [5] T. Dong, W. Liu, M. Ma, H. Peng, S. Yang, J. Tao, C. He, L. Wang, P. Wu, T. An, Hierarchical zeolite enveloping Pd-CeO₂ nanowires: an efficient adsorption/catalysis bifunctional catalyst for low temperature propane total degradation, *Chem. Eng. J.* 393 (2020) 124717.
- [6] S. Song, Q. Liu, J. Xiong, M. Wen, T. An, Promotional effects of Ag on catalytic combustion of cyclohexane over PdAg/Ti-SBA-15, *J. Catal.* 421 (2023) 77–87.
- [7] M. Wen, S. Song, W. Zhao, Q. Liu, J. Chen, G. Li, T. An, Atomically dispersed Pd sites on Ti-SBA-15 for efficient catalytic combustion of typical gaseous VOCs, *Environ. Sci. Nano* 8 (2021) 3735–3745.
- [8] W. Tang, W. Xiao, S. Wang, Z. Ren, J. Ding, P. Gao, Boosting catalytic propane oxidation over PGM-free Co₃O₄ nanocrystal aggregates through chemical leaching: a comparative study with Pt and Pd based catalysts, *Appl. Catal. B: Environ.* 226 (2018) 585–595.
- [9] A. Yang, V. Streibel, T. Choksi, H. Aljama, B. Werghi, S. Bare, R. Sánchez-Carrera, A. Schäfer, Y. Li, F. Abild-Pedersen, M. Cargnello, Insights and comparison of structure–property relationships in propane and propene catalytic combustion on Pd- and Pt-based catalysts, *J. Catal.* 401 (2021) 89–101.
- [10] H. Peng, T. Dong, S. Yang, H. Chen, Z. Yang, W. Liu, C. He, P. Wu, J. Tian, Y. Peng, X. Chu, D. Wu, T. An, Y. Wang, S. Dai, Intra-crystalline mesoporous zeolite encapsulation-derived thermally robust metal nanocatalyst in deep oxidation of light alkanes, *Nat. Commun.* 13 (2022) 295.
- [11] H. Xu, N. Yan, Z. Qu, W. Liu, J. Mei, W. Huang, S. Zhao, Gaseous heterogeneous catalytic reactions over Mn-based oxides for environmental applications: a critical review, *Environ. Sci. Technol.* 51 (2017) 8879–8892.
- [12] R. Yang, Y. Fan, R. Ye, Y. Tang, X. Cao, Z. Yin, Z. Zeng, MnO₂-based materials for environmental applications, *Adv. Mater.* 33 (2021) 2004862.
- [13] Y. Xie, Y. Yu, X. Gong, Y. Guo, Y. Guo, Y. Wang, G. Lu, Effect of the crystal plane figure on the catalytic performance of MnO₂ for the total oxidation of propane, *CrystEngComm* 17 (2015) 3005–3014.
- [14] S. Rong, P. Zhang, F. Liu, Y. Yang, Engineering Crystal facet of α-MnO₂ nanowire for highly efficient catalytic oxidation of carcinogenic airborne formaldehyde, *ACS Catal.* 8 (2018) 3435–3446.
- [15] L. Chen, J. Jia, R. Ran, X. Song, Nickel doping MnO₂ with abundant surface pits as highly efficient catalysts for propane deep oxidation, *Chem. Eng. J.* 369 (2019) 1129–1137.
- [16] S. Wu, H. Liu, Z. Huang, H. Xu, W. Shen, O-vacancy-rich porous MnO₂ nanosheets as highly efficient catalysts for propane catalytic oxidation, *Appl. Catal. B: Environ.* 312 (2022) 121387.
- [17] Y. Yue, J. Fu, C. Wang, P. Yuan, X. Bao, Z. Xie, J. Bassett, H. Zhu, Propane dehydrogenation catalyzed by single Lewis acid site in Sn-Beta zeolite, *J. Catal.* 395 (2021) 155–167.
- [18] C. Zhang, Y. Lan, Y. Cao, S. Tang, Y. Chen, W. Tang, Catalytic combustion of propane over Mg-modified Co_{1.5}Mn_{1.5}O₄ spinel catalysts: boosting C-H cleavage with Lewis acid and oxygen vacancies, *Fuel* 339 (2023) 127140.
- [19] Y. Jian, M. Tian, C. He, J. Xiong, Z. Jiang, H. Jin, L. Zheng, R. Albilali, J. Shi, Efficient propane low-temperature destruction by Co₃O₄ crystal facets engineering: unveiling the decisive role of lattice and oxygen defects and surface acid-base pairs, *Appl. Catal. B: Environ.* 283 (2021) 119657.
- [20] L. Li, X. Feng, Y. Nie, S. Chen, F. Shi, K. Xiong, W. Ding, X. Qi, J. Hu, Z. Wei, L. Wan, M. Xia, Insight into the effect of oxygen vacancy concentration on the catalytic performance of MnO₂, *ACS Catal.* 5 (2015) 4825–4832.
- [21] Y. Jian, Z. Jiang, C. He, M. Tian, W. Song, G. Gao, S. Chai, Crystal facet engineering induced robust and sinter-resistant Au/α-MnO₂ catalyst for efficient oxidation of propane: indispensable role of oxygen vacancies and Au species, *Catal. Sci. Technol.* 11 (2021) 1089–1097.
- [22] M. Polverejan, J. Villegas, S. Suib, Higher valency ion substitution into the manganese oxide framework, *J. Am. Chem. Soc.* 126 (2004) 7774–7775.
- [23] W. Si, Y. Wang, Y. Peng, J. Li, Selective dissolution of A-site cations in ABO₃ perovskites: a new path to high-performance catalysts, *Angew. Chem. Int. Ed.* 54 (2015) 7954–7957.
- [24] C. He, Y. Wang, Z. Li, Y. Huang, Y. Liao, D. Xia, S. Lee, Facet engineered alpha-MnO₂ for efficient catalytic ozonation of odor CH₃SH: oxygen vacancy-induced active centers and catalytic mechanism, *Environ. Sci. Technol.* 54 (2020) 12771–12783.
- [25] L. Zhu, J. Wang, S. Rong, H. Wang, P. Zhang, Cerium modified birnessite-type MnO₂ for gaseous formaldehyde oxidation at low temperature, *Appl. Catal. B: Environ.* 211 (2017) 212–221.
- [26] J. Huang, S. Zhong, Y. Dai, C. Liu, H. Zhang, Effect of MnO₂ phase structure on the oxidative reactivity toward bisphenol A degradation, *Environ. Sci. Technol.* 52 (2018) 11309–11318.
- [27] J. Zhou, L. Qin, W. Xiao, C. Zeng, N. Li, T. Lv, H. Zhu, Oriented growth of layered-MnO₂ nanosheets over α-MnO₂ nanotubes for enhanced room-temperature HCHO oxidation, *Appl. Catal. B: Environ.* 207 (2017) 233–243.
- [28] K. Ye, K. Li, Y. Lu, Z. Guo, N. Ni, H. Liu, Y. Huang, H. Ji, P. Wang, An overview of advanced methods for the characterization of oxygen vacancies in materials, *Trend Anal. Chem.* 116 (2019) 102–108.
- [29] P. Hu, Z. Amghouz, Z. Huang, F. Xu, Y. Chen, X. Tang, Surface-confined atomic silver centers catalyzing formaldehyde oxidation, *Environ. Sci. Technol.* 49 (2015) 2384–2390.
- [30] Y. Yang, J. Huang, S. Zhang, S. Wang, S. Deng, B. Wang, G. Yu, Catalytic removal of gaseous HCBz on Cu doped OMS: effect of Cu location on catalytic performance, *Appl. Catal. B: Environ.* 150–151 (2014) 167–178.
- [31] Y. Yang, J. Huang, S. Wang, S. Deng, B. Wang, G. Yu, Catalytic removal of gaseous unintentional POPs on manganese oxide octahedral molecular sieves, *Appl. Catal. B: Environ.* 142–143 (2013) 568–578.
- [32] F. Hao, Y. Gao, J. Liu, R. Dudek, L. Neal, S. Wang, P. Liu, F. Li, Zeolite-assisted core-shell redox catalysts for efficient light olefin production via cyclohexane redox oxidative cracking, *Chem. Eng. J.* 409 (2021) 128192.
- [33] F. Wang, H. Dai, J. Deng, G. Bai, K. Ji, Y. Liu, Manganese oxides with rod-, wire-, tube-, and flower-like morphologies: highly effective catalysts for the removal of toluene, *Environ. Sci. Technol.* 46 (2012) 4034–4041.
- [34] T. GARCIA, B. SOLSONA, S.H. TAYLOR, The catalytic oxidation of hydrocarbon volatile organic compounds, *Handb. Adv. Methods Process. Oxid. Catal.* 61 (2014).
- [35] J. Zhong, Y. Zeng, M. Zhang, W. Feng, D. Xiao, J. Wu, P. Chen, M. Fu, D. Ye, Toluene oxidation process and proper mechanism over Co₃O₄ nanotubes: Investigation through in-situ DRIFTS combined with PTR-TOF-MS and quasi in-situ XPS, *Chem. Eng. J.* 397 (2020) 125375.
- [36] G. Li, N. Li, Y. Sun, Y. Qu, Z. Jiang, Z. Zhao, Z. Zhang, J. Cheng, Z. Hao, Efficient defect engineering in Co-Mn binary oxides for low-temperature propane oxidation, *Appl. Catal. B: Environ.* 282 (2021) 119512.
- [37] E. Wu, X. Feng, Y. Zheng, D. Lin, Y. Luo, Y. You, B. Huang, Q. Qian, Q. Chen, Inverse coprecipitation directed porous core-shell Mn–Co–O catalyst for efficient low temperature propane oxidation, *ACS Sustain. Chem. Eng.* 8 (2020) 5787–5798.
- [38] Y. Fang, H. Li, Q. Zhang, C. Wang, J. Xu, H. Shen, J. Yang, C. Pan, Y. Zhu, Z. Luo, Y. Guo, Oxygen vacancy-governed opposite catalytic performance for C₃H₆ and C₃H₈ combustion: The effect of the Pt electronic structure and chemisorbed oxygen species, *Environ. Sci. Technol.* 56 (2022) 3245–3257.
- [39] Q. Li, J. Shang, T. Zhu, Physicochemical characteristics and toxic effects of ozone-oxidized black carbon particles, *Atmos. Environ.* 81 (2013) 68–75.

- [40] I. Son, S. Kwon, J. Park, S. Lee, High coke-resistance MgAl₂O₄ islands decorated catalyst with minimizing sintering in carbon dioxide reforming of methane, *Nano Energy* 19 (2016) 58–67.
- [41] W. Dose, S. Donne, Manganese dioxide structural effects on its thermal decomposition, *Mater. Sci. Eng. B. Adv.* 176 (2011) 1169–1177.
- [42] W. Tong, J. Wang, X. Du, X. Wang, Y. Wang, Y. Zhang, Tributyl phosphate degradation and phosphorus immobilization by MnO₂: reaction condition optimization and mechanism exploration, *J. Hazard. Mater.* 432 (2022) 128725.
- [43] S. Kelzenberg, N. Eisenreich, S. Knapp, A. Koleczko, H. Schuppler, H. Fietzek, Chemical kinetics of the oxidation of manganese and of the decomposition of MnO₂ by XRD and TG measurements, *Propellants Explos. Pyrotechnol.* 44 (2019) 714–724.
- [44] M. Taylor, W. Zhou, T. Garcia, B. Solsona, A. Carley, C. Kiely, S. Taylor, Synergy between tungsten and palladium supported on titania for the catalytic total oxidation of propane, *J. Catal.* 285 (2012) 103–114.
- [45] S. Kanitkar, M. Abedin, S. Bhattacharyya, J. Spivey, Methane dehydroaromatization over molybdenum supported on sulfated zirconia catalysts, *Appl. Catal. A: Gen.* 575 (2019) 25–37.
- [46] S. Müller, Y. Liu, M. Vishnuvarthan, X. Sun, A. van Veen, G. Haller, M. Sanchez-Sánchez, J. Lercher, Coke formation and deactivation pathways on H-ZSM-5 in the conversion of methanol to olefins, *J. Catal.* 325 (2015) 48–59.